International Research Journal of Multidisciplinary Scope (IRJMS), 2025; 6(1):1261-1279 IRJMS

Original Article | ISSN (O): 2582-631X DOI: 10.47857/irjms.2025.v06i01.02469

Quantitative Assessment of Brain Tumor Epilepsy by AI Models

Jayanthi Vajiram*, Sivakumar S

Vellore Institute of Technology, Chennai, India . *Corresponding Author's Email: jayanthi.2020@vitstudent.ac.in

Abstract

Epilepsy disorder characterized by recurrent seizures, which is common in 60%-88% of patients with diffuse low-grade gliomas, especially those in superficial cortical or insular regions. Understanding the connection between tumor morphology and epileptogenicity helps to refine diagnostic approaches and support therapeutic interventions. Identifying genetic clusters based on individual genetic profiles, supports to improve the epilepsy treatment methods. The study found the volume of white matter, grey matter, and cerebral spinal fluid in relation to epilepsy occurrence and severity. The preprocessing steps of skull stripping, feature scaling by k-means clustering, and radiomic feature selection by logistic regression models were analyzed. The CNN classifier was used to interpret the data to calculate the volumes of white matter (WM), gray matter (GM), and cerebrospinal fluid (CSF) volumes by marching cube algorithm. The performance metrics are calculated by machine learning (ML) classifiers like Support vector machine (95%), Logistic Regression (91%), AdaBoost (89%), Gaussian Naïve Base (87.5%), Gradient Boost (87%), and deep learning (DL) classifiers like CNN (96%) and DNN (79%). The study used classifiers to assess the accuracy and effectiveness of brain structures by prediction models. Although limited by dataset size, it offers valuable insights into epilepsy disorders with radiomic features. Future research should focus on multimodal analysis, and real-time data integration for improved diagnostic. This is the baseline study in the classification of brain tumor epilepsy (BTE) for upcoming research. Over all study aims to quantitatively assess the relationship between brain tumor morphology and epilepsy using deep learning models applied to MRI data.

Keywords: Canny Edge Algorithm, Deep Learning Models, Machine Learning Models, Marching Cube Algorithm, Volumetric Analysis.

Introduction

Brain tumor epilepsy is a condition causing recurrent seizures that affects patients' quality of life, cognitive function, mobility, and overall well-being. Identifying the cause and treatment is complex, and characterization is crucial for understanding the pathophysiology effects. The end-of-life phase epilepsy can be challenging to describe, and the link to focal cortical dysplasia is complex due to the morphological features and different modalities of brain tumor's structure (1-9). This paper presents a 3D reconstruction approach for BTE image visualization, utilizing preprocessing methods like skull stripping, feature scaling, radiomic cluster selection, and classification. The volumetric analysis by marching cubes algorithm, which creates a 3D surface mesh for segmented regions, aiding in structural abnormality detection, and localization of seizure onset zones, by classification models. The method also includes k-means clustering-based segmentation and semi-automatic threshold selection techniques for accurate classification (10-13). The study evaluates the image detection using clustering techniques, tumor lesion region features for precise classification (14-16). Radiomics method of analyzing tumor phenotypes by extracting high-dimensional quantitative features from image. This noninvasive approach allows for the analysis of tumor characteristics, comparable to molecular biological method of genomics. Several studies have explored the use of radiomics on MRI images to predict the grades of gliomas based on their feature selection methods (17-19). The volumetric analysis in epilepsy image involves skull stripping and the marching cube algorithm. Skull stripping isolates brain structures, while the marching cube algorithm reconstructs brain volume surfaces. This allows for detailed 3D analysis of structural abnormalities. The classification performance metrics was calculated by AI models.This gives the deeper understanding

(Received 17th September 2024; Accepted 27th January 2025; Published 31st January 2025)

and relationship between brain tumor and epilepsy.classification performance metrics was calculated by AI models. This gives the deeper understanding,and relationship between brain tumor and epilepsy.The study can significantly improve the patient care and clinical outcomes by assessing BTE unique characteristics and patterns. This paper provides the analysis of related literature, materials and methods, results, and a conclusion sections. Figure 1 explains the overview of BTE, Figure 2A and 2B explains the visualization of BTE (Dicom & NifTi) images,Figure 3 explains the proposed methodology.

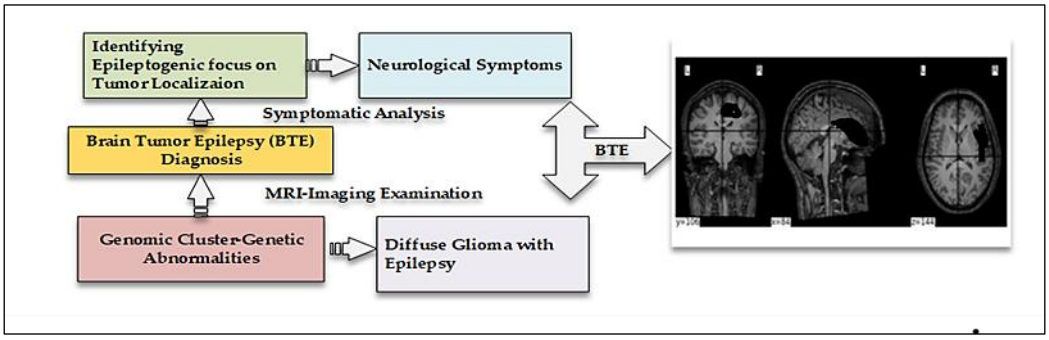

Figure 1: Brain Tumor Epilepsy and Their Causes

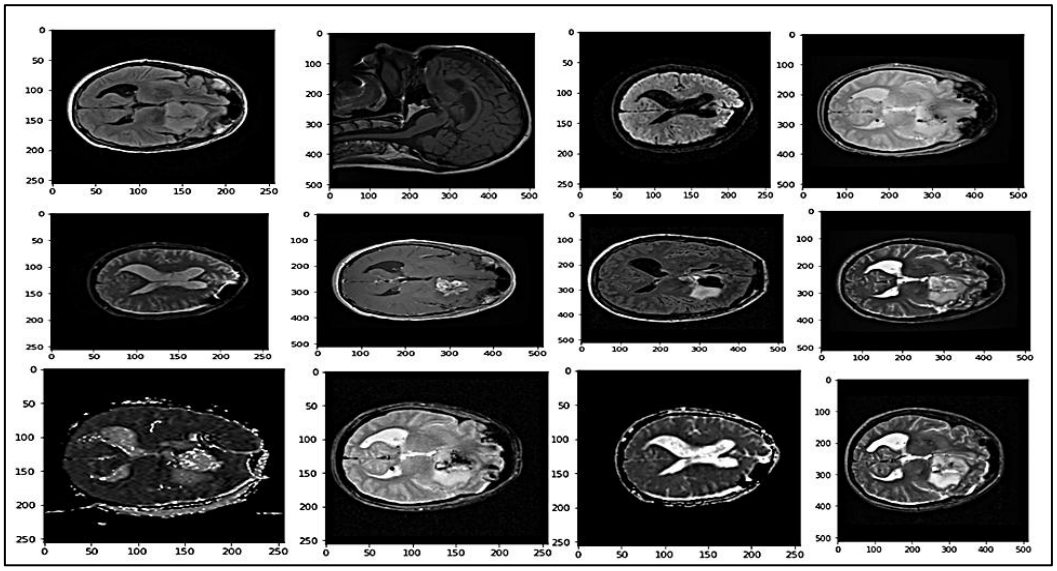

Figure 2: (A) Structural Analysis of BTE Images (DICOM)

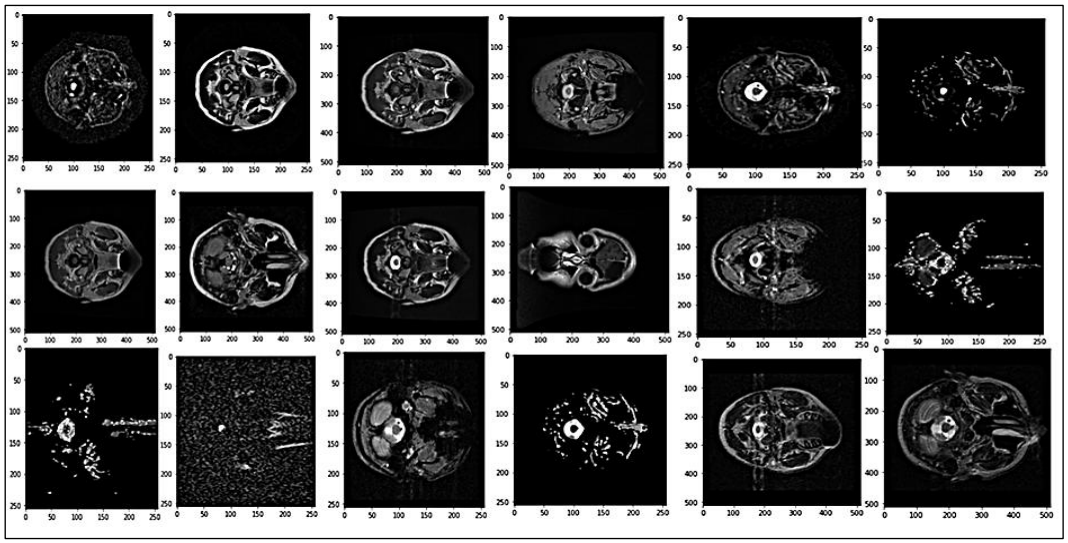

Figure 2: (B) Structural Analysis of BTE Images(NifTi)

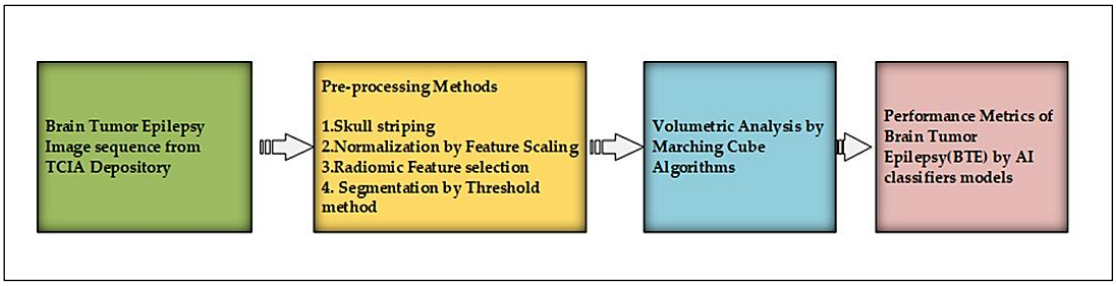

Figure 3: Proposed Methodology

Relative Studies

Recent advancements in deep learning and machine learning have significantly improved the identification of Brain Tumor Epilepsy (BTE), with this section reviewing machine learning and deep learning methods. Artificial intelligence (AI) in neuroimaging reduces errors and increases efficiency, and aid the physician could provide the better patient care. In practice, data artifacts might compromised by ML/DL models performance, AI algorithms could be used for better analysis. AI enhances neuro-oncologists' proper treatment plans. It aids MRI images for automated segmentation and classification of tumor related disease through biomarker method. ML uses algorithms to recognize patterns to make predictions. Supervised learning method using labelled input data to trains algorithms, while unsupervised learning using unlabelled data. Deep learning, analyze data in a logical form similar to brain function, and process raw input data directly. AI used to detect traumatic brain injury , long-term outcomes, and intracranial pressure (20-24). AI used to detect non-linear, non-stationary, low frequency of complex brain signals, and artifacts. It provides clinically relevant information accurately. Clinical analysis of brain tumor and epilepsy is crucial for saving lives. AI, gives time-consuming, and accurate diagnosis ,and increasing in clinical practise for automated detection, lesion prediction, disease progression by improving image quality. Brain-computer interface method gives information about a patient's health condition, mitigate illness stages, by smart medical tools at homes (25, 26).

Machine Learning Methods

Machine learning methods like Logistic Regression, Gradient Boost, Ada Boost, Naïve Bayes, and SVM can classify tumor enlargement using labeled data. Ensemble learning techniques like Ada Boost, and Gradient Boost were used to improve the performance of the model (27-30). The feature scaling and clustering of RNA-seq is a model-based K-means clustering algorithm that addresses issues in unsupervised clustering of single cell RNA-seq samples. The method uses a finite mixture of regression to identify cluster-discriminatory genes and account for potential confounding variables. The methodology used are normalization, candidate gene selection, by logistic regression algorithm (31, 32).

Deep Learning Methods

Neural networks, a deep learning technique mimicking human brain structure, provide better accuracy in BTE classification. The proposed brain tumor classification model based on CNN. The CNN model extracts both global and local features from two parallel stages, addressing over fitting issues. Detecting and classifying these tumors accurately is challenging due to their complex structure. The study used an improved fine-tuned model using CNN, on the BTE datasets (33-36). These methods highlight tubular structures, smooth noise, preserve edges, segment structures, and calculate volume. They are useful for visualizing and analyzing complex structures in images. The marching cube algorithm by CNN model used for analyzing volumetric data. However, it may require fine-tuning and optimization for large datasets and may not differentiate between types or assess epilepsy severity. AI models for these conditions may require large training data, which can be challenging and time-consuming are the limitation of this method.

Methodology

This section, provides the dataset used in the study and discuss the overall system architecture. Figure 3 provides a representation of the model architecture. The various AI algorithms, including XG Boost, AdaBoost, Gaussian, Naïve Bayesian, KNN, SVM, LR, CNN and DNN, used for the detection of BTE and volumetric analysis.

Data Acquisition

The dataset used from the TGCA database, which is a publicly accessible database. The study aims to evaluate the brain tumor epilepsy (BTE) and its relationship with MRI sequences, and other biomarkers. The dataset consisted of 265 subjects, with 105 having BTE and 155 serving as normal controls.

Preprocessing

Pre-processing steps are necessary for preparing input data for proper classification results, by skull stripping, feature scaling, radiomic feature selection. To transform 3D MRI data into 2D slices enables such as gaussian smoothing, which helps in reducing noise and enhancing the clarity of the images.

Skull Stripping Method

Skull stripping and morphological structuring techniques were employed to eliminate non-brain tissue and unwanted sections such as the scalp, skull, and dura from MRI images. The was shown in the Figure 4.

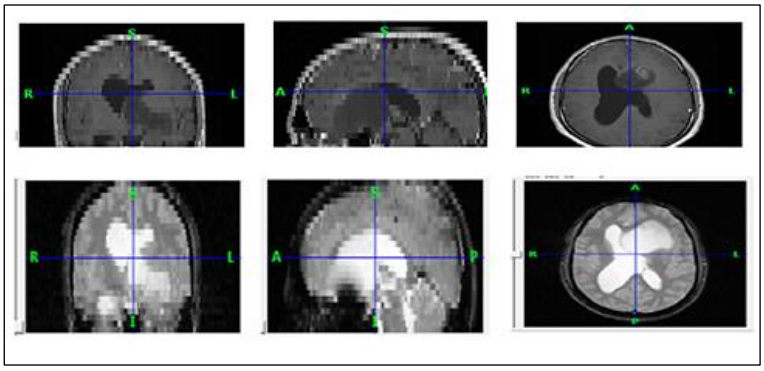

Figure 4: Skull Stripping Process

Machine Learning Approach

Feature Scaling and Radiomic Feature Selection

Feature scaling is a preprocess technique used in volumetric analysis to normalize and standardize input data, ensuring all features have similar scales or magnitudes. This helps in comparing measurements and considering all features equally by min-max [0-1] scaling and standardization. The k-means clustering technique divides images into clusters based on features like intensity, texture, and shape. Feature scaling is used to find intrinsic groups within the unlabeled dataset and draw inferences. The algorithm iterates between many steps until a predetermined stopping criteria is met, such as no data points changing the clusters, minimal distances, or a maximum number of iterations (37-39).The study uses cluster assignment methods to identify groups of brain tumor epilepsy with similar profiles across multiple omic data types. These methods include RNA Seq cluster, which assigns tumor samples based on RNA sequencing data, and methylation cluster, which classifies tumors causing epilepsy with similar methylation, miRNA, CN, and RPPA clusters, which helps to classify BTE and study the correlation between data types and patient survival. The results show the effectiveness of feature selection methods in removing low variance threshold features and providing insights into radiomic cluster patterns by logistic regression model (40-42).

Machine Learning Classifier Models

KNN is a lazy learner algorithm that assigns objects to classes with the most k nearest neighbors, without making assumptions about data distribution. Gaussian Naive Bayes is a probabilistic classifier that uses the Bayes theorem to estimate the likelihood of a test object belonging to each class. Support vector machines (SVM) is used for regression, classification, and outlier detection in n-dimensional spaces. AdaBoost and XG Boost are an ensemble learning algorithm that combines multiple weak learner models to create a strong model. ML models offer accurate classifications and predictions, but require larger sample sizes and are criticized for poor transparency. They divide unlabeled data into labelled groups, aiding human resource improvement and maximizing the benefits (43-45).

Deep Learning Approach

Brain tumor epilepsy is serious disorder, requiring accurate diagnosis for treatment. A deep learning model with a large training cohort can

overcome accuracy limitations and develop a clinically relevant prediction model (46, 47). CNN and DNN are deep learning models used in image recognition, and particularly for MRI classification for brain tumor epilepsy. CNNs analyze and extract features from images, while DNNs provide a comprehensive understanding of data through multiple layers and complex connection.

Segmentation by Threshold Method

Canny edge detection is used in MRI processing to accurately identify and extract boundaries of anatomical structures or areas of interest from the image. This helps in segmentation and subsequent analysis of specific regions.Hessian matrix analysis is employed to detect and characterize the shape and orientation of structures within the MRI data. It provides information about local intensity variations and spatial relationships, aiding in feature extraction and classification.Eigen vector calculations are utilized to compute the principal directions of local image gradients. It gives the information of local geometry and anisotropy of image features. The canny edge algorithm, used in edge detection, is proposed to implement an improved Sobel operator, and iterative threshold filter method. The algorithm enhances noise resistance and preserves useful edge information by suppressing false edges (48-51). The canny edge detection method, used for noise reduction, intensity gradient calculation, non-maximum suppression, and double threshold. Noise reduction is done using gaussian smoothing to eliminate interference. The intensity gradient is calculated using filters and sobel operators. Non-maximum suppression thins out edges, ensuring local maximums are preserved. Double threshold classifies edges based on gradient magnitudes above [0.15] or below [0.1] a threshold. While it can be used in conjunction with deep learning algorithms for various tasks, The noise reduction is applied through a 5x5 gaussian filter with a [2k+1] x [2k+1]kernel size, as stated in equation 1.

$$H_{ij} = \frac{1}{2\pi\sigma^2}\ exp\ exp\ \left(-\frac{(i-(k+1)^2)+(j-(k+1)^2)}{2\pi\sigma^2}\right);\ 1 \le i,j \le (2k+1) \quad [1]$$

The gradient of the image can be calculated by convolving I(*Ix, Iy)* with Sobel kernels Kx and Ky. These kernels use edge and pixel intensity to detect the edges of the image

Kx = [-1 0 1; -2 0 2; -1 0 1]: Ky = [-1 -2 -1; 0 0 0; 1 2 1] [2]

Then, the magnitude G and the slope θ of the gradient are calculated in equation 3 and 4

$$\text{Gradient Intensity } |G| = \sqrt{I_x^2 + I_y^2} \quad [3]$$

$$\text{Edge direction } \theta(x,y) = arctan\frac{I_x}{I_y} \quad [4]$$

Hessian Metric and Eigen Values of the Images

The Hessian matrix is a 2D image symmetric matrix representing the real eigenvalues of an orthogonal coordinate system. It is used to describe second-order image intensity variations and determine the direction of the gradient curve. The process involves smoothing the image using a Gaussian function, convolution masks, and analyzing the gradient of a loss function. The eigenvalues of the Hessian matrix can be used to minimize loss in segmentation tasks. The image can be filtered using a filtering mask, resulting in the partial derivative of the 2D images.Then, numerical approximations are applied to obtain the partial derivatives; Ixx, Iyy, and Ixy.The gaussian function G (x, y) applied as a smoothing function, the equations for Gxx, Gyy and Gxy are constructed by convolution masks for Ixx, Iyy and Ixy. Therefore, in order to obtain Ix, the image can be filtered using the below functions. filtering mask can be generated and convolving the image with x, y = [-3 Σ(sigma):3 Σ], that mask gives the partial derivative of the 2D images as shown in figure 5 , and discused in below equations.

The Gaussian function of the Image $G(x,y,\sigma) = \frac{1}{2\pi\sigma^2}e^{-\frac{(x^2+y^2)}{2\sigma^2}}$ [5]

Taking its partial derivative in x ,y gives Gx :

$$\frac{\partial G(x,y,\sigma)}{\partial x} = -\frac{x}{2\pi\sigma^4}e^{-\frac{(x^2+y^2)}{2\sigma^2}}, Gy : \frac{\partial G(x,y,\sigma)}{\partial y} = -\frac{x}{2\pi\sigma^4}e^{-\frac{(x^2+y^2)}{2\sigma^2}} \quad [6]$$

The equation of Gxx is given by $\frac{\partial^2 G(x,y,\sigma)}{\partial^2 x} = \left(-1+\frac{x^2}{\sigma^2}\right)\frac{e^{-\frac{(x^2+y^2)}{2\sigma^2}}}{2\pi\sigma^4}$ [7]

The equation of Gyy is given by $\frac{\partial^2 G(x,y,\sigma)}{\partial^2 y} = \left(-1 + \frac{y^2}{\sigma^2}\right) \frac{e^{-\frac{(x^2+y^2)}{2\sigma^2}}}{2\pi\sigma^4}$ [8]

The equation of Gxy is given by $\frac{\partial^2 G(x,y,\sigma)}{\partial xy} = \left(\frac{xy}{2\pi\sigma^6}\right) e^{-\frac{(x^2+y^2)}{2\sigma^2}}$ [9]

To apply a gaussian filter to the image using a desired kernel size and standard deviation. This helps to smooth the image and suppress noise.To calculate the partial derivatives of the smoothed image with respect to x and y, and sum up the elements of the hessian matrix to obtain the curvature values at each pixel location. . The eigenvalues represent the curvature along the principal directions, providing information about the type of features like edge or corner, at that location. To calculate the eigenvalues λ_{max} *and* $\lambda_{min}$of the hessian matrix and determine the edge and corner points based on their values. If λ_{max} *and* λ_{min} are positive or negative, it indicates an edge. If both λ_{max} *and* λ_{min} are positive and above a certain threshold, it indicates a corner.These values are determining edge and corner points may vary slightly depending on the specific implementation or algorithm being used.

Hxx = (Ixx * k^2) * Gxx, Hxy = (Ixy * k^2) * Gxy, Hyy = (Iyy * k^2) * Gyy and H = Hxx + Hyy [10]

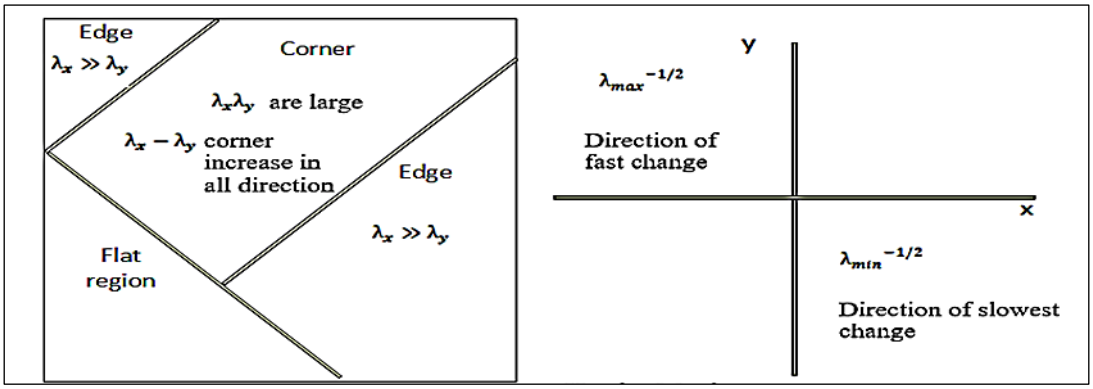

Figure 5: Hessian Metric and Eigen Values of the Images

Marching cube Algorithms

CNN models are used for volumetric data analysis. The model can automatically learn features from the volumetric data and make accurate predictions. The marching cubes algorithm processes the volumetric data on a grid and determines the configuration of the surface within each grid cell, resulting in a mesh that represents the surface. The algorithm undergoes validation through various steps, including testing with diverse input datasets of extreme cases, verifying its accuracy, visualizing the final mesh, and comparing results. This process ensures the algorithm's ability to handle complex geometries and unusual scenarios. The mathematical technique used to create three-dimensional surfaces from data points. It partitions data into cubes, each containing data points or values. The algorithm traverses each cube, examining its values at its eight corners, to determine the object's surface. It can also be used to analyze volumetric data, calculate statistical measures, and generate a surface mesh from 3D voxel intensity data. This technique is commonly used for visualizing complex structures within volumetric data, which is useful in analysis of medical images. The mathematical expression of dividing a 3D volume into voxel grids involves discretizing the volume into discrete elements representing points in 3D space. For example, dividing a volume into N_x, N_y, and $N_z$voxels, the dimensions of each voxel are calculated.

$\Delta_x = \frac{N_x}{X_{max}}$, $\Delta_y = \frac{N_y}{Y_{max}}$, $\Delta_z = \frac{N_z}{Z_{max}}$ are explained as follows [11]

$$X_i = i.$$
$$where\ i = 0,1, \ldots \ldots,$$
$$Y_j = j.$$
$$where\ j = 0,1, \ldots \ldots,$$

$$Z_k = k.$$
$$where\ k = 0,1, \ldots \ldots,$$
$$f(,f(,y_j,),y_{j+1},)f(,y_{j+1},) \quad [12]$$

Let's consider a cube defined by its corner points at indices (i,j,k) where i,j,k are integers representing the indices along the x, y, and z axes, respectively. The intensity values at the corners of this cube can be denoted as f(x,y,z) where x=x_i, y= $y_j$and k= z_k.Here, $f(,y_j,)$represents the intensity value at the corner with indices (i,j,k) and similar notations apply to the other corners. The indices i+1, j+1, k+1 represent the next indices along the respective axes. It uses a cube with 8 vertices and 12 edges as a volume element. A case lookup table stores possible triangulations, with 256 possible subjects of BTE, and abnormality clearly deducted in to 105 cases. An index is created for each case based on vertex intensity. Linear interpolation calculates triangle vertices positions on cell edges, determining surface intersections and interpolating surface intersections along edges . The value is 1 if intensity $\geq$ iso value, and the value is 0 if intensity$<$ iso value. T is a threshold value that determines if a corner is detected or not, based on the intensity of the corner at a specific location. Its value depends on the desired sensitivity.

Intersection=Any corner intensity $\geq$ T or Any corner intensity$<$ T

$$f(x_i,y_j,z_k) \geq T\ or\ f(x_{i+1},y_j,z_k) \geq T\ or \ldots \ldots \ldots \ldots \ldots \ldots or\ f(x_{i+1},y_{j+1},z_{k+1}) < T$$
$$x_{intersection} = x\ ) \quad [13]$$
$$f(x_{i,}y_{i,}z_i) \geq T\ for\ i = 1,2, \ldots .8 \quad [14]$$
$$p_{i=}p_a + \frac{(T-f_a)}{(f_b-f_a)}\ p_a\ ) \quad [15]$$

The volume of a $V_{voxel} = (voxel\_size\_x\ ) * (voxel\_size\_y\ ) * (voxel\_size\_z\ )$ [16]

The cube's corners' intensity values must meet a threshold to intersect the iso-surface. If true for at least one corner, the cube intersects, and its intersection points are calculated. Let T be the threshold intensity level and i_1 and i_2 be two corners of the cube with intensities $f and\ f$where $i_1 <$. These two corners straddle the iso-surface. The co-ordinates of these corners are $x\ and\ x$ .To calculate the X intersection, point along the x-axis where the iso-surface crosses the edge between i_1 and i_2 . The equation interpolates corners $i_1$and $i_2$based on threshold T and intensity values. The algorithm determines if the cube intersects the iso-surface, evaluating if the corners cross the threshold. The representation of a single voxel cube defined by its eight corners (vertices) with intensities f(x,y,z) where x,y and z are the spatial coordinates. If all vertices are above the threshold or all are below, the cube doesn't intersect the iso-surface. If there's a mix of values above and below the threshold, the cube intersects. If a cube intersects, the algorithm proceeds to calculate intersection points and form triangles. Intersection points can be calculated by linearly interpolating between vertices based on the threshold. The $p_i$is the intersection point between vertices p_a and p_b, and $f_a$and $f_b$are their corresponding intensity values. The 3D reconstruction of MRI images has limitations due to factors like artifacts, speckle noise, and suboptimal image quality can affect accuracy and reliability. To analyze the soft tissue data, to reconstruct the 3D models, triangulate the cube configuration by the marching cube algorithm, which is robust under data and threshold values (52-56). The figure 6 shows the random samples of marching cubes. The process of segmenting and classifying structures can be subjective, and can limit real-time applicability. Despite these challenges, 3D reconstruction holds potential benefit for medical education, and to improve methodology and algorithms.

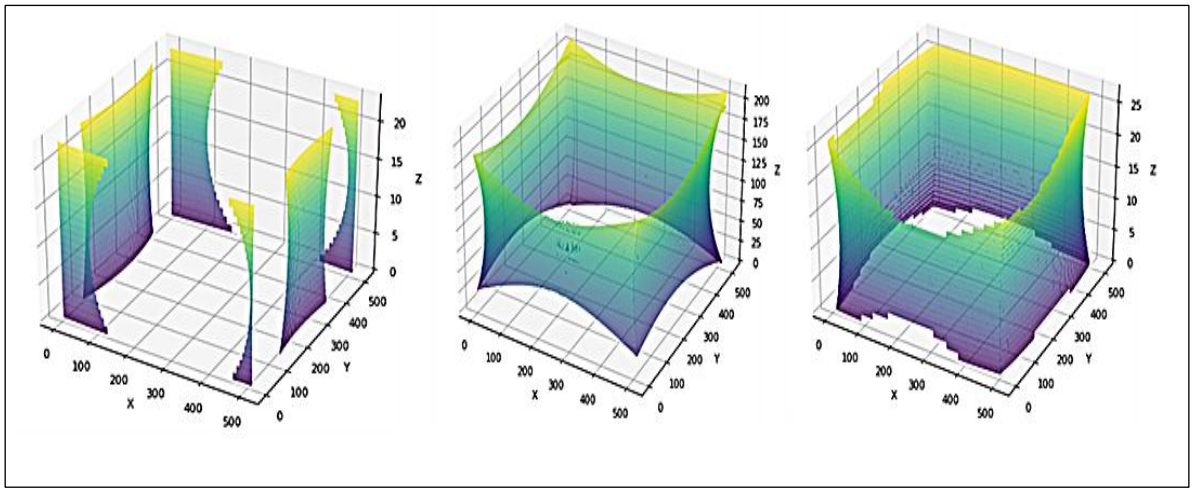

Figure 6: Structure of Marching Cubes

Results and Discussion

This study uses only the MRI images for skull stripping, feature scaling, feature selection and then apply the marching cubes algorithm used for surface extraction from volumetric data for visualization purposes and the voxel intensity data to generate a surface mesh. The classification scores are calculated by different classifier models.

Environmental Setup

The recommended approach is executed on a Windows 10 center i7-4710MQ computer chip running at 2.5 GHz (8 central processors), with 8 GB of Slam and 1 GB of committed illustrations handling unit memory. All experiments are performed on a Personal computer with Intel Core i5 GH z processor and 8.00 GB RAM, nvidia. The proposed method is implemented in Python 3.6.5 with libraries like pydicom, Dicom2nifti, simple ITK, nibabel, nilearn, scipy.ndimage,numpy and matplotlib.pyplot .Import nibabel, skimage.measure, marching cubes, numpy, mayavi, mlab; install Xvfb, create visualization, loop through saved OBJ files, loop through meshes, create visualization of marching cube visualization of images, sklearn.metrics import accuracy score, sklearn import model_selection,sklearn.ensemble,SVC , logistic regression, tensorflow.keras.models import Sequential , Voting Classifier, imblearn.over_sampling.

Analysis of Feature Scaling

This normalization method ensures that each cluster is evaluated on the same scale (0-1). Feature scaling can also reduce the computational complexity of the analysis. Table 1 presents summary statistics for each cluster in the dataset, including cluster, count, mean, standard deviation, minimum, 25th percentile, median, 75th percentile, and maximum. It provides cluster number, count, mean, standard deviation, min, max, and 25th, 50th, and 75th percentile values. Table 2 converts the features in to numerical cluster equivalent. Table 3 provides the feature scaling of the dataset clusters involves normalizing the data so that all of the clusters have the same range of values from 0 to1.

Table 1: Statistical Summary of Cluster Numerical Variables

Variables	RNA Seq Cluster	Methy Lation Cluster	Mirna Cluster	CN Cluster	RPPA Cluster	Oncosign Cluster	COC Cluster	Histological_Type	Neoplasm_ Histologic_ Grade	Laterality	Tumor_ Location	Gender	Age_At_Initial_ Pathologic	Race	Ethnicity	Diagnosis
Count	110	110	110	110	110	110	110	110	110	110	110	110	110	110	110	110
Mean	2.04545	3.645	1.9	1.690	2.1090	1.809091	1.7636	2.109091	1.518182	0.990909	1.99090	3.48	45.418182	2.85454	1.8272	0.24545
std	1.41022	1.215	0.7893	0.885	1.2946	0.760196	0.8559	0.870995	0.519912	0.095346	1.00909	1.88	14.412267	0.48531	0.5394	0.43232
min	0	0	1	0	0	0	1	0	0	0	0	0	0	0	0	0
25%	1	3	1	1	1	1	1	1	1	1	1	2	33.25	3	2	0
50%	2	4	2	1	2	2	1	2	2	1	2	2	46.5	3	2	0
75%	3	5	2	3	3	2	3	3	2	1	3	6	57.75	3	2	0
max	4	5	4	3	4	3	3	3	2	1	3	6	75	3	2	1

Table 2: Features are Converted in to Numerical Cluster Equivalent

Number Of Clusters	RNA Seq Cluster	Methy Lation Cluster	Mirna Cluster	CN Cluster	RPPA Cluster	Oncosign Cluster	COC Cluster	Histological_Type	Neoplasm_ Histologic_ Grade	Laterality	Tumor_ Location	Gender	Age_At_Initial_ Pathologic	Race	Ethnicity	Diagnosis
1	2	4	2	0	3	2	1	2	1	3	2	F	3	2	1	2
2	1	5	1	1	2	1	1	2	1	3	2	M	2	0	1	1
3	1	5	1	2	2	1	1	2	1	1	2	F	3	0	0	1
4	0	5	1	2	1	1	1	1	1	3	6	F	3	0	0	0
5	4	5	1	2	3	1	1	2	1	1	6	F	3	0	0	4

Table 3: Feature Scaling and Normalization

Feature Series	Rna Seq Cluster	Methy Lation Cluster	Mirna Cluster	Cn Cluster	Rppa Cluster	Oncosign Cluster	Coc Cluster	Histological_Type	Neoplasm_ Histologic_ Grade	Laterality	Tumor_ Location	Gender	Age_At_Initial_ Pathologic	Race	Ethnicity	Death01
1	0.5	0.8	0.3333	0.666	0	1	0.5	0.33333	1	1	1	0.33	0	1	1	1
2	0.25	1	0.3333	0.333	0.25	0.66666	0	0.33333	1	1	1	0.33	1	0.6666	0	1
3	0.25	1	0.3333	0.333	0.5	0.66666	0	0.33333	1	1	0.3333	0.33	0	1	0	0
4	0	1	0.3333	0.333	0.5	0.33333	0	0.33333	0.5	1	1	1	0	1	0	0
5	1	1	0.3333	0.333	0.5	1	0	0.33333	1	1	0.3333	1	0	1	0	0

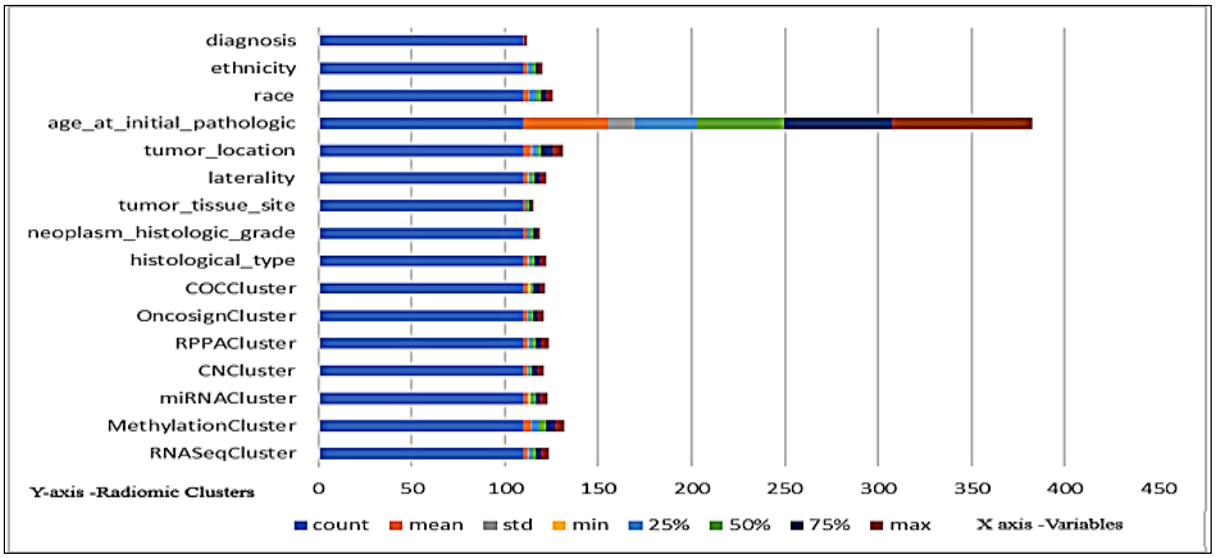

Figure 7: Statistical Value of Clusters

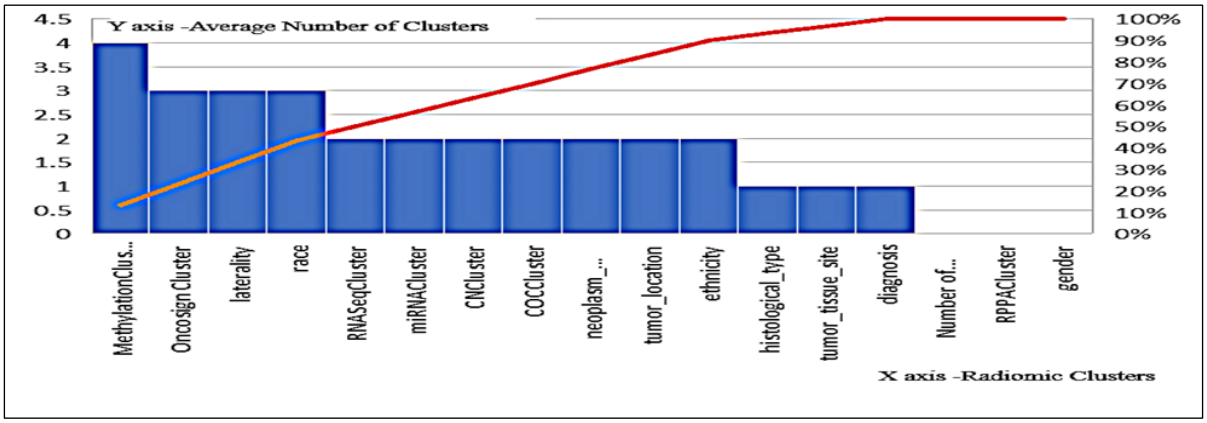

Figure 8: Numerical Equivalent of Clusters

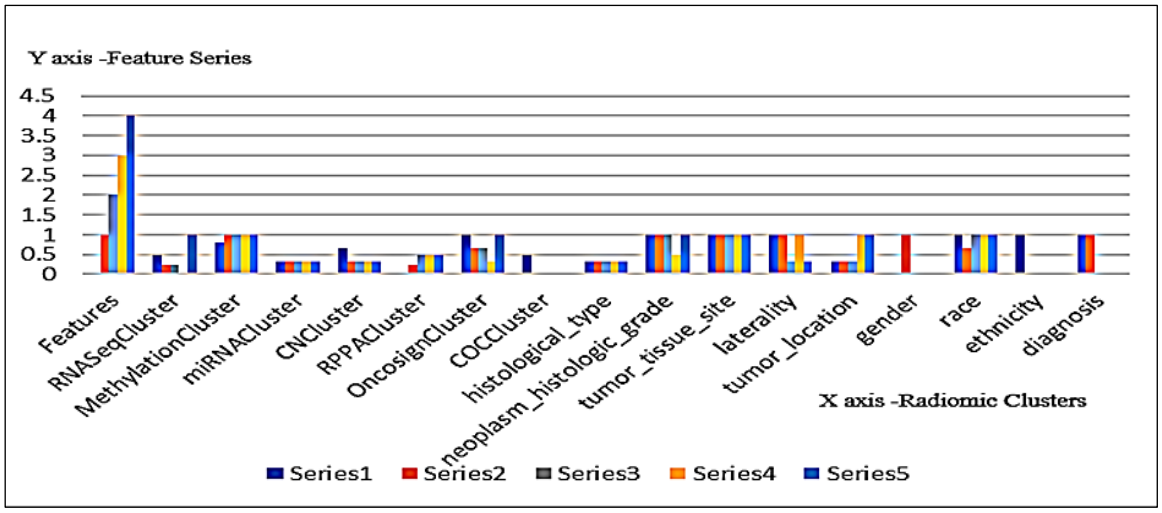

Figure 9: Feature Scaling and Normalization

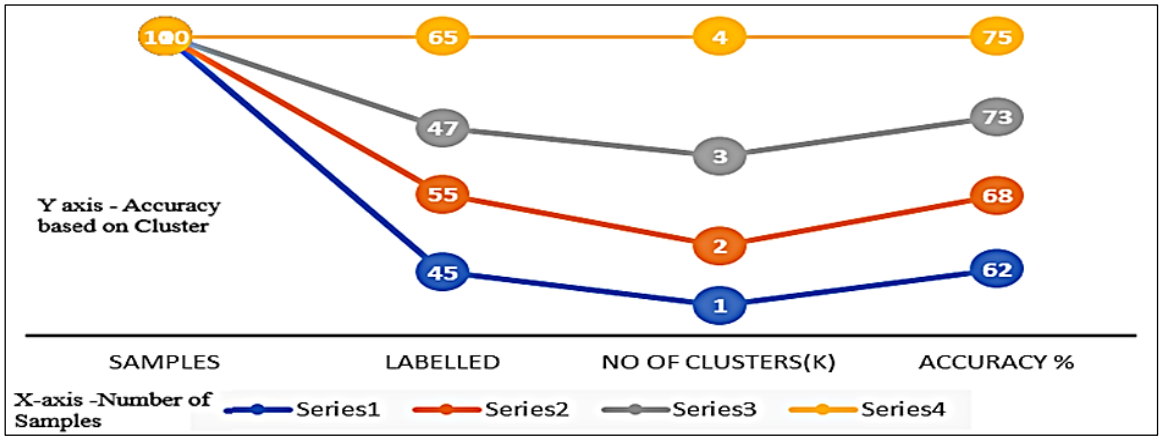

Figure 10: K-means Clustering Model

Figure 7 shows feature scale performance based on statistical value and numerical clusters with k means clusters. This value is determined by calculating the distance between the points within a cluster and the centroid of the cluster. The closer the points are to the centroid, the higher the value of the cluster. Figure 8 shows a numerical value can be used to describe the clusters in terms of size, shape, and density. Figure 9 is a graphical representation of the feature scaling process, which is used to normalize data by transforming it so that all the features have a similar range of values. This allows the data to be more easily clustered. Figure 10 is a graphical representation of a K-means model with different clusters. The graphical representation shows how the data is distributed among the clusters (k=1,40, k=2,55, k=3,41 and k=4,61-labelled) in which k=4 gives better accuracy of 75% (with k means. inertia_ 141.611) better the model to fit.

Analysis of Radiomic Feature Selection

The feature selection methods used to remove low variance threshold features and identifying informative features by regression model. The use of cluster analysis also provided insights into radiomic cluster patterns. Table 4 explains the use of radiomic cluster patterns in identifying Brain tumor epilepsy groups based on consensus clustering of multiple omics data types. It also discusses the use of RNASeqCluster, MethylationCluster, RPPACluster, and cosignCluster. It also discusses the classification of tumors into different types, neoplasm_histologic_grade, laterality, and death01 columns, which can be used to study the correlation between data types and patient survival. These features help in identifying tumors with similar profiles of epilepsy as shown in the Table 4 and Figure 11.

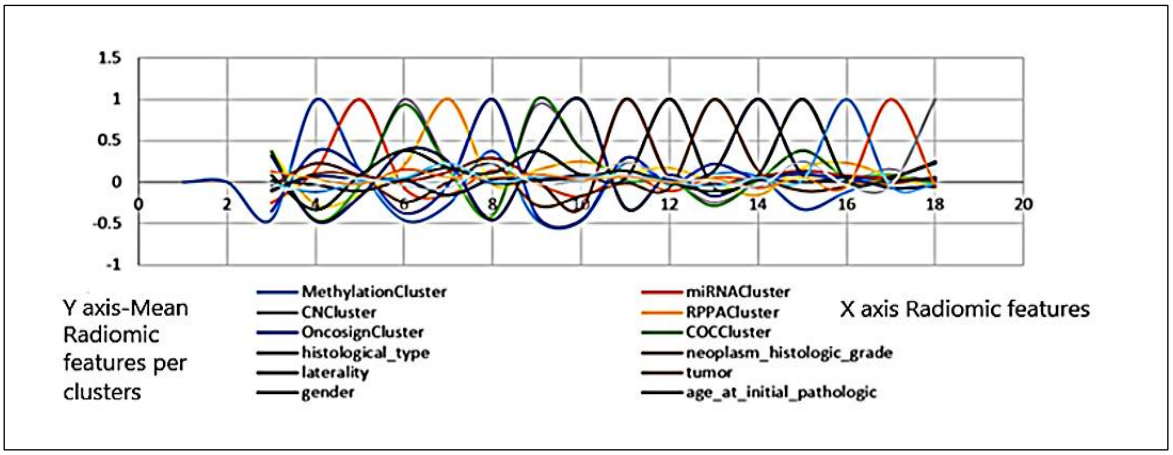

Figure 11: Radiomic Clusters or Features in the BTE Image

Table 4: Radiomic Clusters (features) Selection by Logistic Regression Model

Correlation Clusters	RNA of Seq Cluster	Methy Lation Cluster	Mirna Cluster	CN Cluster	RPPA Cluster	Oncosign Cluster	COC Cluster	Histological_ Type	Neoplasm _Histologic _Grade	Laterality	Tumor_ Location	Gender	Age_At_Initial_ Pathologic	Race	Ethnicity	Death 01
RNASeqCluster	1.000 00	-0.451	-0.249158	0.37	0.3654	-0.35505	0.3	0.319204	-0.040613	1.974972e-02	-0.10965	-0.09	0.085413	-0.0271	1.6e-01	-0.12
MethylationCluster	-0.451	1.000	0.144451	-0.4	-0.271	0.375692	-0.461	-0.471102	0.228920	-3.215368e-02	0.10196	0.06	-0.330874	-0.1192	4.8e-02	-0.03
miRNACluster	-0.249	0.144	1.000000	-0.6	-0.149	0.146218	-0.021	-0.172747	0.089771	-1.044166e-01	0.06047	0.03	0.087339	-0.0007	-2e-02	0.04
CNCluster	0.3701	-0.461	-0.068748	1.00	0.2016	-0.37727	0.9374	0.389947	0.015696	3.588479e-02	-0.24466	0.02	0.383790	0.05091	1.4e-01	-0.04
RPPACluster	0.3654	-0.271	-0.149690	0.20	1.0000	-0.02801	0.1433	0.247407	0.126008	1.682782e-01	-0.00179	-0.15	0.175342	0.23063	6.1e-02	-0.06
OncosignCluster	-0.355	0.375	0.146218	-0.37	-0.028	1.000000	-0.408	-0.459396	0.291861	-1.153338e-02	0.21922	0.03	0.113125	-0.0033	5.3e-02	0.22
COCCluster	0.3685	-0.461	-0.021729	0.93	0.1433	-0.40893	1.0000	0.396420	0.028089	2.420822e-02	-0.28502	0.02	0.379823	0.06654	9.9e-02	-0.02
histological_type	0.3192	-0.471	-0.172749	0.38	0.2474	-0.45939	0.3964	1.000000	-0.313660	8.605558e-02	-0.17041	0.04	0.094885	0.05257	3.4e-02	0.03
neoplasm_histologic _grade	-0.040	0.228	0.089771	0.01	0.1260	0.291861	0.0280	-0.313660	1.000000	4.580013e-02	-0.01781	0.06	0.141347	0.08176	6.8e-02	0.23
laterality	0.0197	-0.032	-0.104417	0.03	0.1682	-0.01153	0.0242	0.086056	0.045800	1.000000e+00	-0.06744	0.02	0.002134	0.00597	7.7e-17	0.05
tumor_location	-0.109	0.101	0.060470	-0.2	-0.001	0.219228	-0.285	-0.170419	-0.017819	-6.744575e-02	1.000 00	0.13	-0.107203	-0.0534	4.0e-02	0.01
gender	-0.095	0.069	0.031336	0.02	-0.157	0.034317	0.0248	0.047516	0.066149	2.804565e-02	0.13623	1.00	0.087880	0.05209	-6.e-02	-0.04
age_at_initial_pathologic	0.0854	-0.333	0.08733	0.38	0.1753	0.113125	0.3798	0.094885	0.141347	2.134116e-03	-0.107	0.08	1.000000	0.02263	5.2e-02	0.24

Correlation Clusters	RNA Seq Cluster	Methy Lation Cluster	Mirna Cluster	CN Cluster	RPPA Cluster	Oncosign Cluster	COC Cluster	Histological_ Type	Neoplasm _ Histologic _ Grade	Laterality	Tumor_ Location	Gender	Age_At_Initial_ Pathologic	Race	Ethnicity	Death 01
			0								20					
race		-0.027	-0.119	-0.0007	0.05	0.2306	-0.00334	0.0665	0.052572	0.081760	5.972113e-03	-0.0534	0.05	0.022632	1.00000	-5.e-02	-0.03
ethnicity		0.1310	0.044	-0.02105	0.15	0.0610	0.059886	0.0972	0.034981	0.068384	7.726196e-17	0.04094	-0.06	0.054187	-0.0507	1.e+00	-0.03
death01		-0.120	-0.036	0.04644	-0.4	-0.067	0.225777	-0.020	0.038442	0.239928	5.903994e-02	0.01292	-0.0	0.249853	-0.0368	-3.e-02	1.00

Analysis of Marching Cube Algorithm

The marching cube algorithm takes input in the form of nifty images and produces a volumetric mesh with five components: scalp, skull, csf, gm, and wm. The process involves loading, realigning, and reslicing the input image to create the surface mesh. The surface mesh visualization generates three components: scalp, skull, and brain. The segmentation step refines the images for each component (scalp, skull, csf, gm, wm) to create a mesh (triangulated surface mesh and hexahedral volume mesh) using the marching cube algorithm. The MC algorithm converts the surface and volume rendering of nifty images into 3D data. It works with cubes that have 8 vertices each, resulting in 256 ways a surface can intersect. The algorithm reduces the 256 cases to 25 patterns.The classifiers interact with the volumetric data obtained from the marching cubes algorithm by examining the properties of each voxel in the volume. It creates a grid of voxels, which represent different regions in space. Each voxel contains information such as its position, density, color, or any other relevant property of the object being represented. The CNN classifiers then analyze the voxel data to determine various characteristics or features that are useful for classification purposes. For example, they might look for patterns or structures. The algorithm was applied to the binary masks of GM, WM, and CSF to extract surface meshes. To determine the threshold level for each tissue type, which is corresponds to the desired tissue type. This helps to extract the surface mesh of each tissue type. Prior to applying the marching cubes algorithm, pre-processing steps on the images were in a suitable format for surface reconstruction and visualization was important. After preprocessing, each voxel in the image was assigned to its corresponding radiomic cluster label. This allowed us to label each voxel based on its cluster membership, providing valuable information about the genetic characteristics of the tissue. The resulting surface mesh sequence of images is shown in Figure 12, Figure 13, and Figure 14. These visualizations help to understand the genetic clustering patterns within the brain tissue and provide a visual representation of the genetic characteristics of the brain structure.

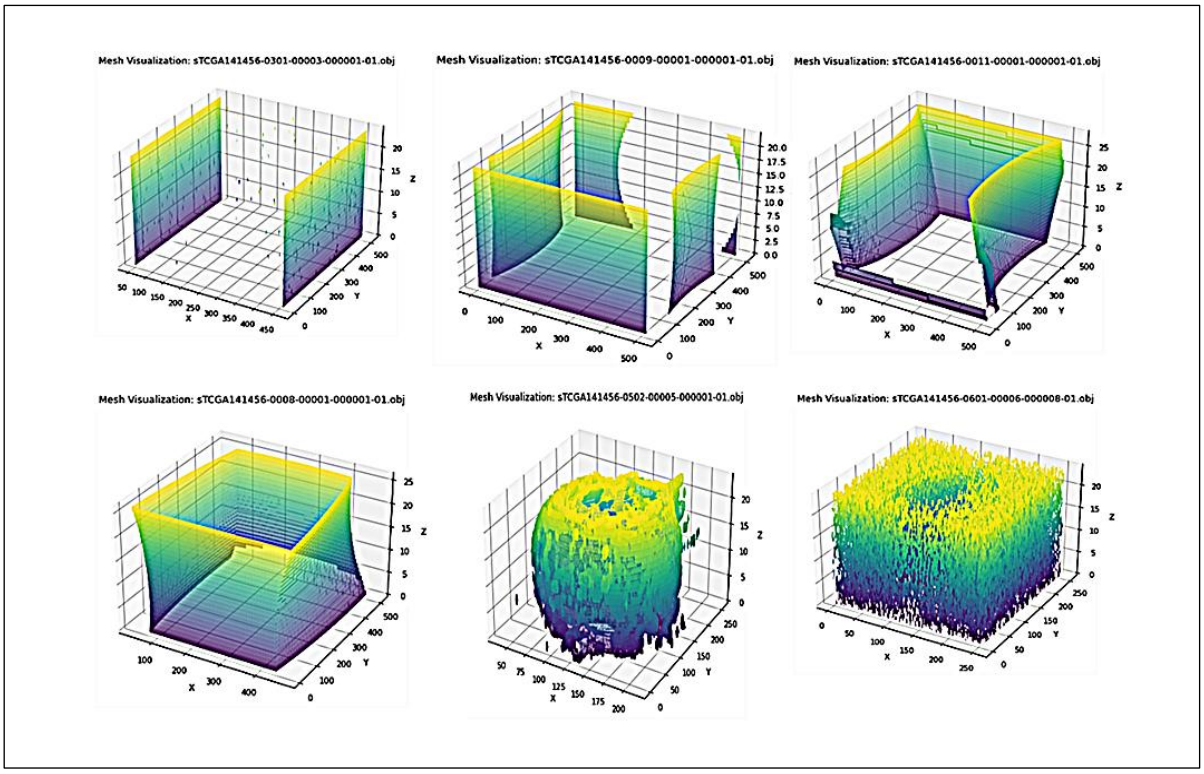

Figure 12: 3D-Mesh Structure of sTCGA141456 Sequence of BTE Images

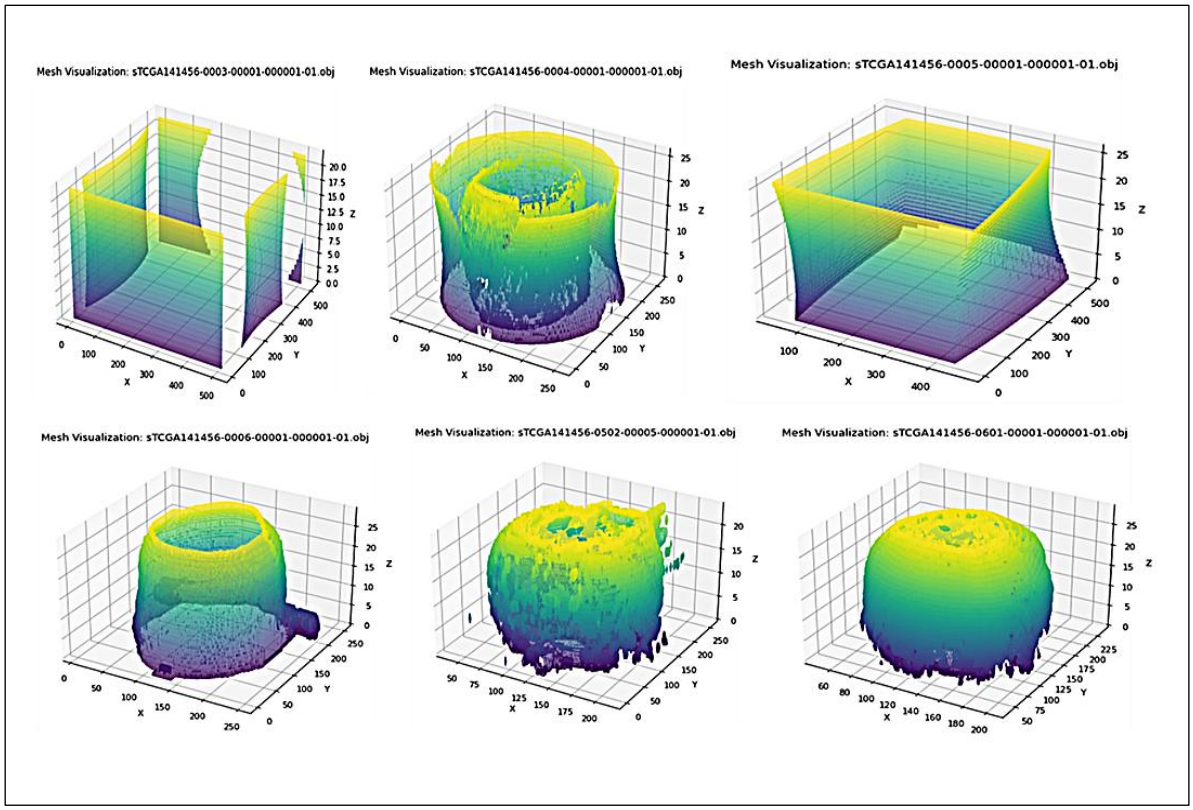

Figure 13: 3D-Mesh Structure of sTCGA141456 Sequence of BTE Images

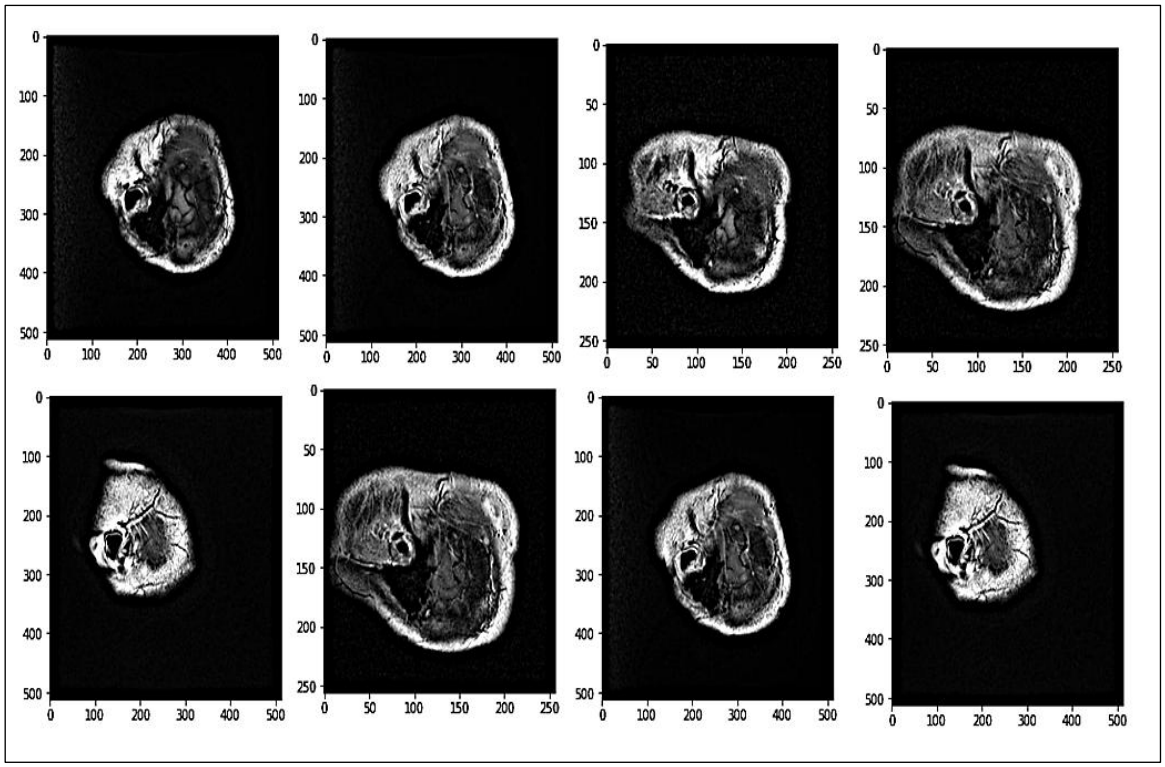

Figure 14: Abnormal Structure Varies from Actual Anatomical Structure

Table 5: Volumetric Analysis of Brain Tumor Epilepsy

Brain Tumor Epilepsy- (DICOM Images are Converted to Nifty format)	**White Matter Volume** mm^3	**Gray Matter Volume** mm^3	**Cerebro Spinal Fluid Volume** mm^3
sTCGA141456-0004-00001-000001-01.nii	759690.32	7905787.76	3045435.02
sTCGA141456-0006-00001-000031-01.nii	637531.25	5418832.64	6342262.36
sTCGA141456-0007-00001-000001-01.nii	859646.80	7466640.09	3484027.51
sTCGA141456-0003-00001-000001-01.nii	561239.84	8177898.56	447756.94
sTCGA141456-0005-00001-000001-01.nii	0860188.01	7581203.09	3369464.51
sTCGA141456-0006-00001-000001-01.nii	5387878.42	5474704.54	6286390.46
sTCGA141456-0201-00002-000001-01.nii	793043.08	8593455.79	31545.64
sTCGA141456-0011-00001-000001-01.nii	295897.71	8059595.30	2816266.55
sTCGA141456-0009-00001-000001-01.nii	900329.96	8178334.90	447320.60
sTCGA141456-0008-00001-000001-01.nii	6985640.53	7585290.70	3365376.90
sTCGA141456-0010-00001-000001-01.nii	311871.31	7466844.31	3483823.28
sTCGA141456-0301-00003-000001-01.nii	890011.75	6299595.89	1635406.45
sTCGA141456-0401-00004-000001-01.nii	183471.68	7155666.18	779333.82
sTCGA141456-0501-00005-000001-01.nii	344707.03	9858997.34	1078502.66
sTCGA141456-0502-00005-000001-01.nii	871276.45	6458094.25	5780984.58
sTCGA141456-0501-00005-000008-01.nii	716513.45	2154015.42	1476905.75
sTCGA141456-0701-00007-000001-01.nii	008502.18	6312205.01	1622797.34
sTCGA141456-0601-00001-000001-01.nii	752751.95	2285519.67	9475575.33

sTCGA141456-0801-00008-000001-01.nii	520266.14	8699268.72	2238228.16
sTCGA141456-0601-00006-000001-01.nii	674894.63	6296141.52	1638860.82
sTCGA141456-0600-00001-000001-01.nii	411994.63	2285519.67	9475575.33
sTCGA141456-0503-00005-000001-01.nii	155171.88	2259247.16	5675752.84
sTCGA141456-0601-00006-000008-01.nii	417046.88	7599992.75	1775007.25
sTCGA141456-1002-00010-000001-01.nii	250482.81	747688.99	5127510.47
sTCGABBA5HY-0008-00060-000001-01.nii	651069.86	3058578.87	1975021.44
sTCGA141456-1001-00010-000001-01.nii	104165.23	6299146.69	1635855.65
sTCGA141456-1201-00012-000001-01.nii	557286.06	8679748.92	2257747.96
sTCGA141456-0901-00009-000001-01.nii	294812.04	6963664.76	19135.24
sTCGA141456-1002-00010-000018-01.nii	289661.02	749165.56	5126033.91
sTCGA141456-1301-00013-000001-01.nii	431876.62	6734861.00	1735139.00
sTCGA141456-1101-00011-000001-01.nii	75590.23	5769166.49	1490833.51
sTCGA141456-1002-00010-000035-01.nii	697092.77	749176.10	5126023.36
sTCGA141456-1002-00010-000052-01.nii	316502.29	749186.65	5126012.82
sTCGA141456-1002-00010-000069-01.nii	488674.61	749006.65	5126012.82
Brain Tumor Epilepsy (DICOM images are converted to Nifty format)	**White Matter Volume** mm^3	**Gray Matter Volume** mm^3	**Cerebro Spinal Fluid Volume** mm^3
sTCGAHT7879-0005-00001-000001-01.nii	651066.98	7362440.56	703280.56
sTCGAHT7879-0012-00001-000001-01.nii	523552.97	1328622.95	1044256.63
sTCGAHT7879-0004-00001-000001-01.nii	524783.45	8100533.83	195622.67
sTCGAHT7879-0006-00001-000001-01.nii	197214.68	13284152.20	1046333.96
sTCGAHT7879-0009-00001-000048-02.nii	560470.84	8059029.64	2311166.36
sTCGAHT7879-0009-00001-000047-01.nii	596924.04	8058985.14	2311210.86
sTCGAHT7879-0008-00001-000001-01.nii	644868.51	3516538.42	54702.17
sTCGAHT7879-0007-00001-000001-01.nii	140817.35	9549643.92	995407.64
sTCGAHT7879-0010-00001-000024-01.nii	419732.27	7951151.90	2419046.35
sTCGAHT7879-0301-00001-000001-01.nii	170048.99	4085183.17	7068245.52

Table 5 explains the brain volume, which was determined by the size of a voxel along each axis, of the affected regions.The average adult human brain having an approximate gray matter volume of 600-700 cm^3, white matter volume is around 400-600 cm^3, and the estimated CSF volume is around $1.5x10^8$ mm^3 to $2x10^8$ mm^3. These values are approximate and can vary based on factors like age, gender, genetics, of individual persons.

Analysis of Classifier Models

The accuracy of a model was determined by the ratio of true positives (TP) to false negatives (TN). Sensitivity, or recall, is the number of accurately predicted positives. An F1-score measures the balance between precision and recall, with precision being the proportion of correctly classified positives. The hyperparameter tuning used to optimize pre-trained models, are learning rate and batch size between 1e-1 and 1e-5 with grid search method. The learning rate $6.2346e^{-0.4}$,batch size 32 and epochs 30. The optimal tuning was achieved by iterating over parameter values within the defined range. In a recent study, researchers used a convolutional

neural network to classify brain tumors using MRI images from public datasets. Their approach achieved an accuracy of 86.23% in one study and 81.6% in another study, outperforming previous methods this study was achieve an accuracy of 96.09% in detecting brain tumor epilepsy using the CNN algorithm (57). The study is a baseline study in the classification of brain tumor epilepsy. This study has significant implications for future research and could potentially help clinicians in accurately detecting and classifying brain tumor epilepsy. Table 6 and Figure 15 explains the Support Vector Machine and CNN Architecture classifiers achieved the highest accuracy for classifying brain tumor epilepsy, with accuracies of 95.83% and 96.09235%. Logistic Regression and Gaussian Naïve Bayes also achieved high accuracies of 91.67% and 87.54%. The DNN Architecture, achieved a lower accuracy of 79.2651%. Overall, the Support Vector Machine and CNN Architecture classifiers are more effective in classifying brain tumor epilepsy than the other classifiers.

Table 6: Performance Metrics of Classifier Models

Machine Learning Classifiers	**Accuracy %**	**Precision**	**Recall**	**F-Measure**
Support Vector Machine	95.83	0.0065	0.99	0.0688
Logistic Regression	91.67	0.003	1.022	0.071
AdaBoost	89.36	0.0586	1.0001	0.0493
Gaussian Naïve Bayes	87.54	0.0094	0.63	0.0687
Gradient Boosting	87.2	0.0956	0.5454	0.1314
Deep Learning Classifiers	**Accuracy %**	**Precision**	**Recall**	**F-measure**
CNN Architecture	96.09235	0.1587203	0.0634625	0.539681
DNN Architecture	79.2651	0.4761511	0.0795612	0.548796

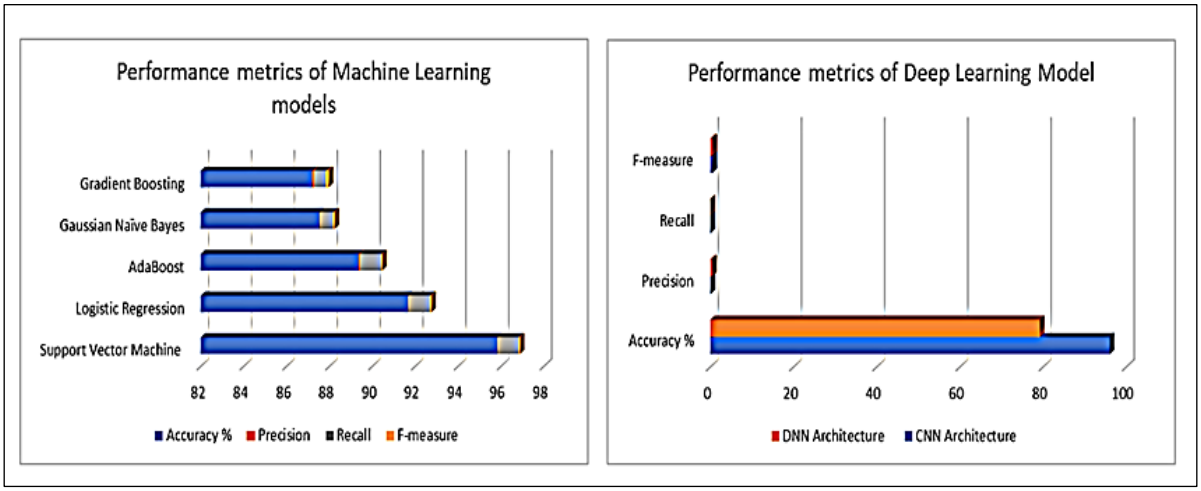

Figure 15: Analysis of Performance Metrics

Conclusion

This study was the baseline for upcoming research and comparative earlier studies are not available. Based on the results of the cluster, volumetric analysis, it is clear that there is distinct relation of genetic clusters in patients with brain tumors and epilepsy. Feature scaling was used to standardize the variables used in the analysis, ensuring that each variable had equal weight and minimizing the impact of outliers. This allowed for a more accurate comparison of the genetic and volumetric data. Overall, the findings suggest that there may be related genetic factors or some common radiomic clusters that contribute to the development and progression of brain tumors and epilepsy treatments. The limitation of marching cube algorithms is mainly used for surface reconstruction and the slice data is affect the stair stepping effect when the surface is paralleled with slices. Existing studies utilize Marching cubes to

quantify tumor volumes. The analysis may simplify the complex factors contributing to epilepsy.Combining multimodal data, such as imaging, genomics, and EEG recordings, could provide a better analysis. In conclusion, the combination of radiomic cluster, volumetric, and performance analysis between brain tumors, epilepsy, and their underlying genetic factors were analyzed. Further research is needed to understand the more related genetic mechanisms involved and to potentially identify the genetic targets of BTE for treating these conditions with large dataset. Real-time clinical data is not pre-processed and this can lead to lower accuracy when using AI models. Additionally, patient reports are typically kept secure and it is difficult to obtain access to them for research purposes. Furthermore, there is a lack of separate open-source datasets specifically focused on epilepsy MRI images, making it challenging to develop accurate models. The implementation should be further enhanced with the real time clinical data to overcome image quality, incorrect parameters, variations in image characteristics, subjectivity in interpretation for accurate prediction and on-time treatment.

Abbrevation

Nil.

Acknowledgement

I acknowledge the support and guidance of Dr. R. Rajeswaran, Head of the Radiology Department, in Sri Ramachandra Medical Research Institute-Chennai. His assistance has been valuable in understanding the concepts more easily.

Author Contributions

All Authors are contributed equally.

Conflict of Interest

The authors declare that they have no conflicts of interest to report regarding the present study.

Ethics Approval

Not applicable.

Funding

None.

References

1. Seidel S, Wehner T, Miller D, Wellmer J, Schlegel U, Grönheit W. Brain tumor related epilepsy: pathophysiological approaches and rational management of antiseizure medication. Neurological Research and Practice. 2022; 4(1):45.
2. Johan AF, Koekkoek. Epilepsy in the end-of-life phase of brain tumor patients: a systematic review. Euro-Oncology Practice. 2014; 1(3):134–140.
3. Slegers RJ, Blumcke I. Low-grade developmental and epilepsy associated brain tumors: a critical update. Acta Neuropathology Communication. 2020; 8(1): 27.
4. Shah GD, Kesari S, Xu R, Batchelor TT, O'Neill AM. Comparison of linear and volumetric criteria in assessing tumor response in adult high-grade gliomas. Neuro Oncology. 2006; 8(1):38-46.
5. Shearkhani O, Khademi A, Eilaghi A, Hojjat S. Detection of Volume-Changing Metastatic Brain Tumors on Longitudinal MRI Using a Semiautomated Algorithm Based on the Jacobian Operator Field. Am J Neuro Radiology (AJNR). 2017; 38(11):2059-2066.
6. Bahadure NB, Ray AK, Thethi HP. Image Analysis for MRI Based Brain Tumor Detection and Feature Extraction Using Biologically Inspired BWT and SVM. Int J Biomed Imaging. 2017; 9749108.
7. Jayanthi V, Sivakumar S. Image enhancement and de-noising techniques of magnetic resonance images.Asian Engineering Journal. 2022;12:137-142.
8. Källberg D, Vidman L, Rydén P. comparison of Methods for Feature Selection in Clustering of High-Dimensional RNA-Sequencing Data to Identify Cancer Subtypes. Front Genet. 2021; 24(12): 632620.
9. Islam MK, Ali MS, Miah MS, Rahman MM, Alam MS, Hossain MA. Brain tumor detection in MR image using superpixels, principal component analysis and template based K-means clustering algorithm. Machine Learning with Applications. 2021 Sep 15;5:100044.
10. Ramtekkar PK, Pandey A and Pawar MK. Accurate detection of brain tumor using optimized feature selection based on deep learning techniques. Multimedia Tools and Application. 2023; 82: 44623–44653.
11. Jibon FA, Khandaker MU, Miraz MH, Thakur H. Cancerous and Non-Cancerous Brain MRI Classification Method Based on Convolutional Neural Network and Log-Polar Transformation. Healthcare (Basel). 2022; 10(9):1801.
12. Joseph SS, Dennisan A. Optimized CNN based Brain Tumor Detection and 3D Reconstruction, Computer Methods in Biomechanics and Biomedical Engineering. Imaging and Visualization.2023; 11(3):796-811.
13. Mehmood I, Sajjad M, Muhammad K, Shah SI, Sangaiah AK, Shoaib M, Baik SW. An efficient computerized decision support system for the analysis and 3D visualization of brain tumor. Multimedia Tools and Applications. 2019 May 30;78:12723-48.
14. Vajiram J, Shanmugasundaram S, Rangasami R, and Maurya U. Comparative Analysis of Seizure Manifestations in Alzheimer's and Glioma Patients via Magnetic Resonance Imaging. Information Dynamic Application. 2023; 2(4): 162-172.
15. Amin J, Sharif M, Haldorai A. Brain tumor detection and classification using machine learning: a comprehensive survey. Complex Intelligence Systems. 2022; 8: 3161–3183.

16. Agustin HP, Hidayati HB, Sooai AG, Purnama IK, Purnomo MH. Volumetric Analysis of Brain Tumor Magnetic Resonance Image. In2019 International Conference on Computer Engineering, Network, and Intelligent Multimedia (CENIM). IEEE. 2019 Nov 19; 1-6.
17. Fekraoui F, Babahenini M. Automatic Marching Cubes for Improving 3D Medical Images Reconstruction. Journal of Digital Information Management. 2020;18(1). Doi: 10.6025/jdim/2020/18/1/1-10
18. Aerts HJ. Decoding tumor phenotype by noninvasive imaging using a quantitative radiomics approach. Nature Communications. 2014; 5: 4006.
19. Gillies RJ, Kinahan PE and Hricak H. Radiomics: Images are more than pictures, they are data. Radiology. 2016; 278:563–577.
20. Monsour R, Dutta M, Mohamed AZ, Borkowski A, Viswanadhan NA. Neuroimaging in the Era of Artificial Intelligence: Current Applications. Fed Pract. 2022; 39(1):S14-S20.
21. Farzad V. Farahani , Krzysztof Fiok *et al* ,Explainable AI: A review of applications to neuroimaging data, Sec. Neural Technology, Front. Neurosc. 2022; 16. Doi: 10.3389/fnins.2022.906290
22. Khalighi S, Reddy K, Midya A. *et al.* Artificial intelligence in neuro-oncology: advances and challenges in brain tumor diagnosis, prognosis, and precision treatment. npj Precis. Onc. 2024 ; 8:80.
23. Sophia Mirkin,Benedict C. Albensi. Should artificial intelligence be used in conjunction with Neuroimaging in the diagnosis of Alzheimer's disease? Front. Aging Neurosci.Sec. Alzheimer's Disease and Related Dementias. 2023; 15. Doi: 10.3389/fnagi.2023.1094233
24. Pierre K, Turetsky J, Raviprasad A, Sadat Razavi S.M *et al,*Machine Learning in Neuroimaging of Traumatic Brain Injury: Current Landscape, Research Gaps, and Future Directions. Trauma Care. 2024; 4:31-43.
25. Xu M,Ouyang Y, Yuan Z. Deep Learning Aided Neuroimaging and Brain Regulation. Sensors. 2023; 23: 4993.
26. Choi KS, Sunwoo L. Artificial Intelligence in Neuroimaging: Clinical Applications. Investig Magn Reson Imaging. 2022; 26(1):1-9.
27. Saidani O, Aljrees T, Umer M, Alturki N, Alshardan A. Enhancing Prediction of Brain Tumor Classification Using Images and Numerical Data Features. Diagnostics (Basel). 2023; 13(15): 2544.
28. Dutta S, Bandyopadhyay PSK. Revealing Brain Tumor Using Cross-Validated NGBoost Classifier. Research Square. 2020; https://europepmc.org/article/ppr/ppr190609.
29. Zhang Hw, Huang Dl, Wang Yr. CT radiomics based on different machine learning models for classifying gross tumor volume and normal liver tissue in hepatocellular carcinoma. Cancer Imaging. 2024; 24: 20.
30. Manikandan P, Durga U and Ponnuraja C . An integrative machine learning framework for classifying SEER breast cancer. Scientific Reports. 2023; 13: 5362.
31. Lim, DK, Rashid NU, Ibrahim JG. Model-based feature selection and clustering of RNA-seq data for unsupervised subtype discovery. Annals of Applied Statistics. 2021;15(1):481-508.
32. Ranjan B, Sun W, Park J. DUBStepR is a scalable correlation-based feature selection method for accurately clustering single-cell data. Nature Communication. 2021; 12: 5849.
33. ZainEldin H, Gamel SA, El-Kenawy EM, Alharbi AH. Brain Tumor Detection and Classification Using Deep Learning and Sine-Cosine Fitness Grey Wolf Optimization. Bioengineering (Basel). 2022;10(1):18.
34. Irmak E. Multi-Classification of Brain Tumor MRI Images Using Deep Convolutional Neural Network with Fully Optimized Framework. Iran J Sci Technol Trans Electrical Eng .2021;45: 1015–1036.
35. Rahman T, Islam MS. MRI brain tumor detection and classification using parallel deep convolutional neural networks. Measurement: Sensors. 2023 Apr 1;26:100694.
36. Asiri AA, Shaf A, Ali T, Aamir M, Irfan M. Brain Tumor Detection and Classification Using Fine-Tuned CNN with ResNet50 and U-Net Model: A Study on TCGA-LGG and TCIA Dataset for MRI Applications. Life. 2023; 13: 1449.
37. Peeken J C, Bernhofer M, Wiestler B, Goldberg T. Radiomics in Radio Oncology - challenging the medical physicist. Physic Medica. 2018; 48: 27–36.
38. Qin JB, Liu Z, Zhang H, Shen C, Wang XC, Tan Y . Grading of Gliomas by Using Radiomic Features on Multiple Magnetic Resonance Imaging (MRI) Sequences. Medical Science Monitor. 2017; 23:2168-2178.
39. H. -h. Cho, H. Park. Classification of low-grade and high-grade glioma using multi-modal image radiomics features, 39th Annual International Conference of the IEEE Engineering in Medicine and Biology Society (EMBC), Jeju, Korea (South). 2017; 3081-3084.
40. Bae JH, Kim M, Lim JS, Geem ZW . Feature Selection for Colon Cancer Detection Using K-Means Clustering and Modified Harmony Search Algorithm. Mathematics. 2021; 9: 570.
41. Yang P, Huang H. and Liu C. Feature selection revisited in the single-cell era. Genome Biol. 2021; 22: 321 .
42. Efremova, M, Teichmann SA. Computational methods for single-cell omics across modalities. Nature Methods. 2020; 17(1):14–7.
43. Black JE, Kueper JK, Williamson TS. An introduction to machine learning for classification and prediction. Family Practice. 2023; 9:40(1):200-204.
44. Naseeba B, Challa NP, Doppalapudi A, Chirag S, Nair NS. Machine learning models for news article classification. In2023 5th International Conference on Smart Systems and Inventive Technology (ICSSIT). IEEE. 2023 Jan 23:1009-1016.
45. Kolluri J, Razia DS, Nayak SR. Text classification using machine learning and deep learning models. InInternational conference on artificial intelligence in manufacturing & renewable energy (ICAIMRE) 2019 Jun 4. http://dx.doi.org/10.2139/ssrn.3618895
46. Talukder MA, Islam MM, Uddin MA, Akhter A, Pramanik MA, Aryal S, Almoyad MA, Hasan KF, Moni MA. An efficient deep learning model to categorize brain tumor using reconstruction and fine-tuning.

Expert systems with applications. 2023 Nov 15;230:120534.
47. Darmofal M, Suman S, Atwal G, Chen JF, Varghese A, Chang JC, Rema AB, Syed A, Morris Q, Berger M. Deep-learning model for tumor type classification enables enhanced clinical decision support in cancer diagnosis. Cancer Research. 2023 Apr 4;83(7_Supplement):5440.
48. Choi KH, Ha JE. An Adaptive Threshold for the Canny Edge with Actor-Critic Algorithm. IEEE Access. 2023; 11:67058-67069.
49. Wu C, Ma H, Jiang H, Huang Z, Cai Z, Zheng Z, Wong CH. An improved Canny edge detection algorithm with iteration gradient filter. In2022 6th International Conference on Imaging, Signal Processing and Communications (ICISPC). IEEE. 2022 Jul 22; p.16-21. doi: 10.1109/ICISPC57208.2022.00011.
50. Wei D, Ling Y, Zhang W. Canny Edge Detection Algorithm Based on Sparse Representation Denoising. InProceedings of the 2022 6th International Conference on Electronic Information Technology and Computer Engineering. 2022 Oct 21; 1707 – 1712.
51. Maksimovic V, Petrovic M, Savic D, Jaksic B, Spalevic P. New approach of estimating edge detection threshold and application of adaptive detector depending on image complexity. Optik. 2021 Jul 1;238:166476.
52. Lee Y, Lee JM, Park SH. Three-dimensional soft tissue landmark detection with marching cube algorithm. Scientific Reports. 2023; 13: 1544.
53. Wang X, Gao S, Wang M, Duan Z. A marching cube algorithm based on edge growth. Virtual Reality & Intelligent Hardware. 2021 Aug 1;3(4):336-49.
54. Ouyang, Jinwu and Zhang, Guijin and Cao, Peizhi and Li, Wen, A Three-Dimensional Geological Modelling Method Using a Modified Marching Cubes Algorithm. 2023; 32. http://dx.doi.org/10.2139/ssrn.4624601
55. Lope, A, Brodlie K. Improving the robustness and accuracy of the marching cubes algorithm for iso-surfacing. IEEE Transactions on Visualization and Computer Graphics. 2003; 9(1):16-29.
56. Delibasis KS, Matsopoulos GK, Mouravliansky NA, Nikita, KS. A novel and efficient implementation of the marching cubes algorithm, Computerized Medical Imaging and Graphics. 2001; 25(4):343-352.
57. Kumar S, Kumar D. Human brain tumor classification and segmentation using CNN. Multimedia Tools and Applications. 2023 Feb;82(5):7599-620.